ACS NANO

Cite This: ACS Nano 2018, 12, 6273–6279

www.acsnano.org

ARTICLE

Graphene Oxide–Upconversion Nanoparticle Based Portable Sensors for Assessing Nutritional Deficiencies in Crops

Davide Giust,[†] María Isabel Lucío,[†] Afaf H. El-Sagheer,[‡,§] Tom Brown,[‡] Lorraine E. Williams,[∥,⊥] Otto L. Muskens,[†,⊥] and Antonios G. Kanaras*[,†,⊥]

[†]Physics and Astronomy, Faculty of Physical Sciences and Engineering, [∥]Biological Sciences, Faculty of Natural and Environmental Sciences, and [⊥]Institute for Life Sciences, University of Southampton, Southampton, SO17 1BJ, U.K.

[‡]Department of Chemistry, University of Oxford, Chemistry Research Laboratory, 12 Mansfield Road, Oxford, OX1 3TA, U.K.

[§]Chemistry Branch, Department of Science and Mathematics, Faculty of Petroleum and Mining Engineering, Suez University, Suez 43721, Egypt

Supporting Information

ABSTRACT: The development of innovative technologies to rapidly detect biomarkers associated with nutritional deficiencies in crops is highly relevant to agriculture and thus could impact the future of food security. Zinc (Zn) is an important micronutrient in plants, and deficiency leads to poor health, quality, and yield of crops. We have developed portable sensors, based on graphene oxide and upconversion nanoparticles, which could be used in the early detection of Zn deficiency in crops, sensing mRNAs encoding members of the ZIP-transporter family in crops. ZIPs are membrane transport proteins, some of which are up-regulated at the early stages of Zn deficiency, and they are part of the biological mechanism by which crops respond to nutritional deficiency. The principle of these sensors is based on the intensity of the optical output resulting from the interaction of oligonucleotide-coated upconversion nanoparticles and graphene oxide in the absence or presence of a specific oligonucleotide target. The sensors can reliably detect mRNAs in RNA extracts from plants using a smartphone camera. Our work introduces the development of accurate and highly sensitive sensors for use in the field to determine crop nutrient status and ultimately facilitate economically important nutrient management decisions.

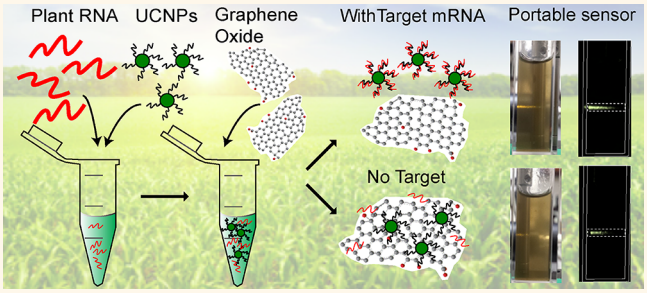

KEYWORDS: *upconversion, nanoparticles, plants, dna, mrna, sensor, graphene oxide*

Micronutrient malnutrition is a global problem and its alleviation is an important challenge to tackling food security concerns. Zinc is a mineral micronutrient and deficiency in humans is widespread, resulting in a whole range of heath defects.[1] Cereal crops are a staple source of food across the world but are low in mineral micronutrients in their edible parts.[2] In addition to low Zn in grain, growth in soils where there is low Zn availability leads to reduced agricultural yield, and so there are consequences for quality and quantity of food. Fertilizer applications to ensure adequate yields is not only expensive but has serious environmental consequences; therefore developing technology to use these more efficiently would be an important advance for sustainable agriculture. Accumulation of mineral micronutrients in plant cells depends on the presence of membrane transporter proteins, and members of several different families have been implicated in Zn transport in crops including metal tolerance proteins (MTPs),[3−6] heavy metal ATPases[7] and ZRT, IRT-related proteins (ZIPs).[8,9] Some of these transporters are upregulated under nutrient stress conditions to ensure more efficient uptake and use of the available nutrients. The sophisticated sensing and response mechanisms responsible for homeostatic control of Zn are starting to be elucidated in cereal crops, and particular members of the ZIP family seem to play a key role as early indicators of Zn-deficiency stress.[8−10]

The ability to monitor or predict plant nutrient status would be a clear advance to the agricultural sector. The development of technology employing state-of-the-art approaches to monitor biomarkers is important for basic research, but could also be applied to monitor crop performance directly in the field and thereby take actions to avoid loss in yield. Most techniques to

Received: May 1, 2018
Accepted: May 31, 2018
Published: June 6, 2018

DOI: 10.1021/acsnano.8b03261
ACS Nano 2018, 12, 6273–6279

detect biomarkers rely on complex laboratory procedures that are often time-consuming and require skilled personnel. For example, the real time polymerase chain reaction (RT-PCR), usually employed for the detection of altered gene expression in various organisms, involves a procedure for the conversion of extracted RNAs into complementary DNAs, requiring a sufficient level of purification of extracts, and then amplification and detection with expensive equipment.[11] Therefore, low-cost and rapid methods for direct detection of biomarkers, without having to implement additional purification and amplification steps are of great interest for a range of applications. In this context, research has been focused on the development of DNA sensors.[12−15] Most types of sensors usually involve the attachment of oligonucleotide sense strands on a functional surface and the output is recorded optically, electrically, or electrochemically upon binding of a complementary target. Among these, optical sensors involving the controlled quenching of fluorescence molecules have been broadly utilized. The most common design involves the incorporation of an energy transfer pair where the fluorescence of a donor organic dye is quenched by an acceptor, typically a surface or another molecule. However, despite their enormous success as labels in a variety of platforms, most commonly used organic dyes exhibit phenomena such as photobleaching and photoblinking, which can strongly hinder their potential. In addition, photoexcitation in the UV−visible region typically introduces nonspecific backgrounds related to autofluorescence of biological environments.[16] In recent years, the development of upconversion lanthanide-doped nanoparticles (UCNPs) has offered an alternative to conventional fluorophores because of their photochemical stability, absence of blinking and photobleaching and, most important, the upconversion mechanism itself that results in a low autofluorescence background when using near-infrared excitation.[17,18] Because of such properties, UCNPs have been successfully employed in a wide range of biomedical applications.[19]

Our group has recently reported the use of hexagonal phase $NaYF_4$:Er^{3+},Yb^{3+} upconversion nanoparticles, functionalized with single-stranded DNAs (UCNPs-ssDNA) for the detection of oligonucleotides with high sensitivity. This assay was first designed to combine the emissive optical properties of UCNPs and the quenching ability of graphene oxide (GO) for the detection of poly-A sequences in the picomolar range.[20] Subsequently, sensors to detect specific mRNA biomarkers present in Alzheimer disease and prostate cancer and optimized for use in blood plasma and cell lysate were developed.[21] GO has been widely reported to act as an effective quencher in various fluorescence-based assays.[22−24] The quenching activity of GO depends on the interactions occurring between the sp^2 hybridized carbon of GO and the aromatic structures and polar groups present in single-stranded oligonucleotides. The working principle of our assay relies on UCNPs-ssDNA interactions with GO in the absence of a complementary oligonucleotide target, through the formation of hydrogen and $\pi-\pi$ stacking interactions between the nucleobases and the aromatic system on GO.[25,26] In the presence of a specific target sequence, the ssDNA on UCNPs is hybridized with its complementary strand, and the UCNPs no longer adsorb to the GO. The intensity of the upconversion fluorescence emitted in the presence or absence of a specific complementary target confirms the presence or absence of the complementary target. In our previous work,[20,21] the output detection of the GO/UCNPs sensors was achieved using laboratory-based grating spectrometers and single-photon counting systems, which precluded the use of these sensors in the field.

Here we describe the development of portable GO/UCNPs sensors for the detection of biomarkers related to the nutrient deficiency in crops. Specifically, we chose to focus on Zn nutrition, detecting the induction of ZIP mRNAs as indicators for Zn deficiency. The portable GO/UCNPs sensors include the use of a smartphone camera as an optical detector and they selectively detect specific mRNAs in a mixture of RNAs. A schematic illustration of the principle of the sensors is shown in Scheme 1. RNA is isolated from crops and mixed with upconversion nanoparticles, which are coated with oligonucleotides designed to hybridize with the target mRNAs. Graphene oxide is added to the solution, and the sample is irradiated with a portable 980 nm laser source. A smartphone camera detects the fluorescent signature of the sample, which confirms the presence or absence of the mRNA target. The advantage of these sensors is not only the portability but also the ability to apply them directly on RNA extracts, eliminating the additional steps for reverse transcription or DNA amplification required by RT-PCR.

Scheme 1. Schematic Illustration of the Detection of mRNA Biomarkers Related to the Nutrient Deficiency in Crops[a]

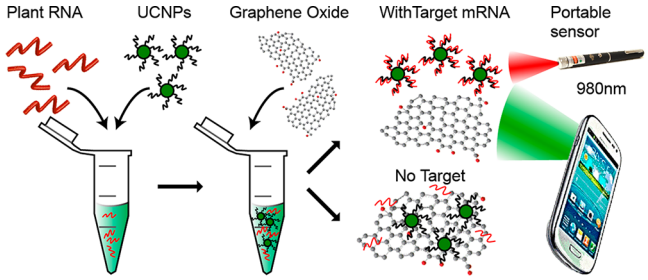

[a]RNA extracts from crops are mixed with oligonucleotide-coated upconversion nanoparticles for a few minutes to allow hybridization of the target sequences. Then, graphene oxide is added, and the sample is irradiated with a portable 980 nm laser source. The fluorescence output is detected by the camera of a smartphone confirming the presence or absence of the target mRNA sequence.

RESULTS AND DISCUSSION

Synthesis and Oligonucleotide Functionalization of Upconversion Nanoparticles. Hexagonal phase $NaYF_4$:Yb^{3+} (25%), Er^{3+} (3%) upconversion nanoparticles (*core UCNPs*) with an average size of 32.1 ± 2.8 nm (Figure 1a,b) were synthesized following a well-established solvothermal method.[27] The core particles of the UCNPs were coated with a $NaYF_4$ shell following a modified method previously reported.[28] The formation of a shell has been shown to result in an increase at the upconversion emission, which is related to a decrease in surface defects of the lattice and concomitantly reduced energy dissipation, as well as to an improved light harvesting, promoted by the shell formation.[29−31] The use of $NaYF_4$:Yb^{3+} (25%), Er^{3+} (3%) @$NaYF_4$ (*core−shell UCNPs*) allows an increase of the upconversion emission and, thus, improves the performance of the sensor.[29] The synthesized core−shell UCNPs exhibited a larger size than the core ones (40.8 ± 3.4 nm, Figure 1c,d), as well as an enhanced fluorescence emission compared to the core UCNPs (Figure 1e), while as expected the upconversion nanoparticles maintained their hexagonal phase after the core−shell

DOI: 10.1021/acsnano.8b03261
ACS Nano 2018, 12, 6273−6279

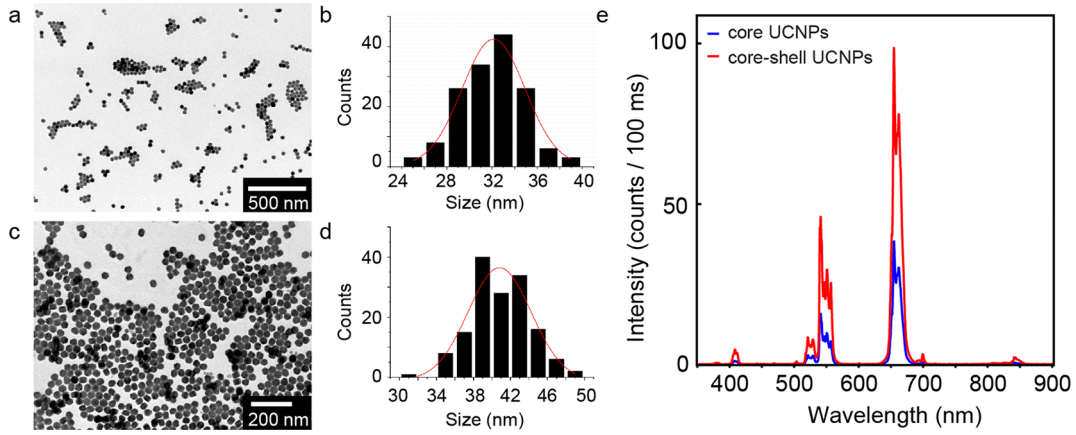

Figure 1. Transmission electron micrographs and nanoparticle size distribution histograms of $NaYF_4$:Yb^{3+} (25%), Er^{3+} (3%) upconversion nanoparticles (*core UCNPs*) (a,b); and $NaYF_4$:Yb^{3+} (25%), Er^{3+} (3%) @$NaYF_4$ (*core−shell UCNPs*) (c,d). (e) Fluorescence emission spectra of core UCNPs (blue line) and core−shell UCNPs (red line).

formation as confirmed by XRD measurements (Supporting Information Figure S1).

The core−shell UCNPs were coated with poly(acrylic acid) (PAA) following a ligand exchange reaction as previously reported.[32] The PAA is hydrophilic, which facilitates the transfer of nanoparticles in water. Moreover, it contains carboxylic groups, which can be functionalized with amine-modified molecules. In our experiments amine-modified sense oligonucleotides strands were coupled to PAA coated core−shell UCNPs using EDC coupling and the successful coupling was confirmed by *Z*-potential and UV−vis spectroscopy (Figure S2) as well as FT-IR (Figure S3). The sense oligonucleotide sequences were designed to be complementary to short oligonucleotide sequences for specific MTP and ZIP mRNAs (Table S1). Members of these families that are implicated in Zn transport were chosen.

Detection of *OsMTP1* mRNA in Transgenic *Arabidopsis* Using a Portable GO/UCNPs Sensor. To test the ability of a portable set up to detect the fluorescence output of our sensors, we first chose to detect the mRNA for the rice Zn transporter protein OsMTP1. For this purpose, we used RNA extracts from three types of plants: *Arabidopsis* wild-type plants (wild-type); *Arabidopsis mtp1-1* mutant that lacks expression of AtMTP1 (*mtp1-1*) and finally *mtp1-1* mutant lines genetically modified to express the rice gene *OsMTP1* under the 35S promoter (*mtp1-1* + *OsMTP1*). Only the latter should show a signal for *OsMTP1* mRNA.[4] For the purpose of our experiment, the upconversion nanoparticles were functionalized with sense strands designed to detect *OsMTP1* mRNA, and they were mixed with the RNA extracts and then graphene oxide was added. As a control experiment, a second batch of nanoparticles was functionalized with sense strands for the detection of *AtACT2* mRNA, a housekeeping gene. The fluorescence output of the solutions was monitored using the portable configuration shown in Figure 2a. The set up consists of a compact 980 nm wavelength laser producing 200 mW of optical power, a cuvette, and a detection system consisting of a collection of lenses, a 900 nm absorptive short-pass filter, and a smartphone with a camera. Figure 2b shows images of the fluorescence output, which were used to obtain the total integrated fluorescence intensity over the entire interaction length in the cuvette. Figure 2c shows the total camera intensity of fluorescence detected for the sensor assays. While for all three types of plants similar levels of *AtACT2* mRNA were

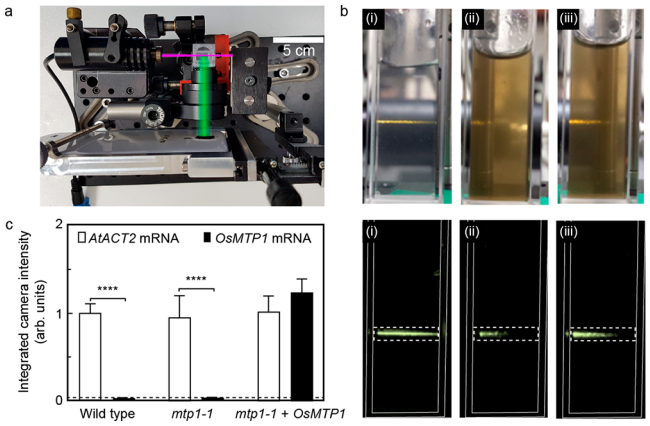

Figure 2. (a) Digital camera image of the portable configuration used to detect the fluorescence output of the sensor. The set up includes a compact arrangement of 980 nm laser, a cuvette, detection optics and a smartphone camera. Magenta and green lines indicate 980 nm laser and detection paths, respectively. (b) Digital camera images under light and in dark showing (i) ssDNA coated core−shell UCNPs (ii) ssDNA coated core−shell UCNPs and GO in the absence of the *OsMTP1* mRNA target and (iii) ssDNA coated core−shell UCNPs and GO in the presence of the *OsMTP1* mRNA target. Dashed lines: area of integration within cuvette boundaries (indicated by thin lines). (c) Integrated camera intensity of the fluorescence output in the presence of different samples corresponding to wild-type *Arabidopsis* plants (Wild type), *mtp1-1* mutant, and *mtp1-1* mutant genetically modified to express the rice gene *OsMTP1*. mRNA expression of the housekeeping gene *AtACT2* is used as a control. One-Way ANOVA and Tukey test analysis. (****) = $p \leq 0.0001$ was applied. Dashed line: background level of the sensor output.

detected, high levels of *OsMTP1* mRNA were only detected in the transgenic *mtp1-1* mutant plants transformed with *OsMTP1*.

Detection of ZIP mRNAs in Barley Using Portable GO/UCNPs Sensors. Detecting biomarkers which are early signs for Zn deficiency is useful in crop management. Having demonstrated the successful detection of the *OsMTP1* mRNA in transgenic *Arabidopsis*, we constructed sensors to evaluate the presence or absence of ZIP mRNAs in barley following exposure to Zn deficiency. First, barley was grown in hydroponics for 7 days in the presence of Zn, and then half

DOI: 10.1021/acsnano.8b03261
ACS Nano 2018, 12, 6273−6279

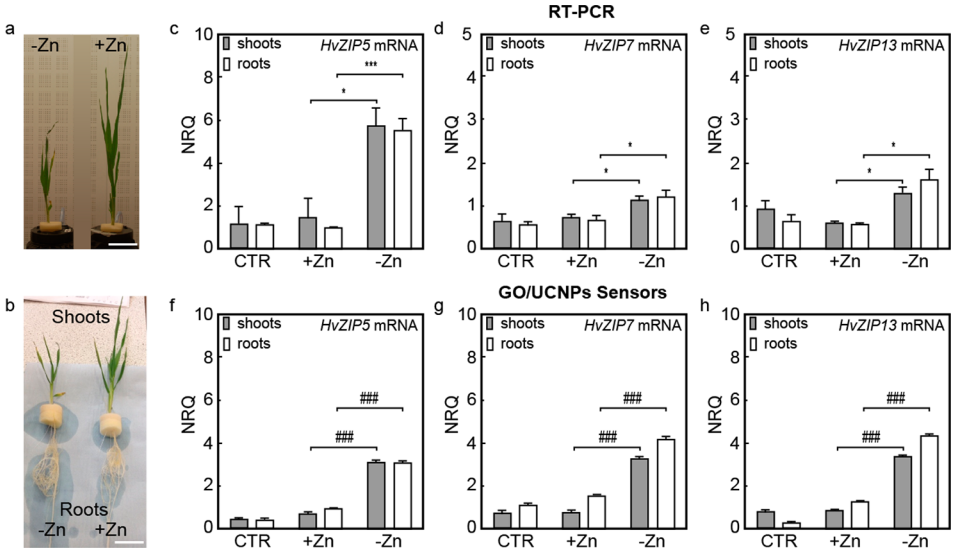

Figure 3. Evaluation of *HvZIP5* mRNA, *HvZIP7* mRNA, and *HvZIP13* mRNA in RNA extracts from barley; (a,b) barley grown for 7 days in the presence of Zn and then another 9 days in the presence or absence of Zn, (+Zn) and (−Zn), respectively. Differences in shoots length and roots network formation are observed. Scale bars, 5 cm; (c−e) detection of cDNAs related to *HvZIP5* mRNA, *HvZIP7* mRNA, and *HvZIP13* mRNA using RT-PCR and (f−h) detection of *HvZIP5* mRNA, *HvZIP7* mRNA, and *HvZIP13* mRNA using portable GO/UCNPs sensors. RNA extracts were taken from plants grown for 7 days in the presence of Zn (CTR) and from plants grown for a further 9 days either in the presence or absence of Zn. All results were normalized to the housekeeping gene *HvACT1*. The mean differences were statistically analyzed by using One-Way ANOVA, Dunnet and Tukey *ad-hoc* post analysis of expression within the same plant total RNA type for the −Zn against the +Zn. (∗) $p \leq 0.05$; (∗∗) $p \leq 0.01$; (∗∗∗∗) $p \leq 0.0001$ (statistics for RT-PCR); (###) $p \leq 0.001$ (statistics for sensor).

of the plants were grown for a further 9 days in the presence of Zn while the other half were grown in the absence of Zn. This was a slightly different time course to that previously reported to induce Zn deficiency,[10] but a similar reduction in shoot biomass was observed under Zn deficiency, as illustrated in Figure 3a,b. RNA was extracted from the roots and shoots of these plants, and it was used to detect the mRNAs for *HvZIP5*, *HvZIP7*, and *HvZIP13*, which are regulated by the presence or absence of Zn in barley.[8,10] To confirm that the relevant mRNAs were present in the extracts, we used RT-PCR to detect the associated complementary DNAs (cDNAs). Figure 3 panels c−e show the data obtained for all three ZIP cDNAs normalized to the cDNA for the housekeeping gene *HvACT1*. Under the time-course used here, we observed an induction of *HvZIP5*, *HvZIP7*, *HvZIP13* for the plants exposed to Zn deficiency; thus indicating they were good candidates to investigate further using the relevant GO/UCNPs sensors. For this purpose, three batches of core−shell UCNPs coated with sense oligonucleotide strands for the detection of *HvZIP5*, *HvZIP7*, and *HvZIP13* mRNAs were synthesized and mixed directly with the RNA extracts of the different plants and then graphene oxide was added. The fluorescent signature of all the different samples was recorded by a smartphone camera using the portable laser configuration shown in Figure 2a. The signals were obtained as integrated camera intensities and were subsequently normalized to the signals of the corresponding *HvACT1* housekeeping gene for each sample, in order to obtain a normalized relative quantification (NRQ) similar to RT-PCR. Again, the ZIPs were seen to be upregulated under Zn deficiency in both roots and shoots (Figure 3f−h). Therefore, the portable sensors constructed here are able to directly detect the barley genes that are up-regulated under Zn-deficiency in a cocktail of RNA extracts, thereby showing promise for future use in the field.

CONCLUSIONS

There is great potential in the application of nanotechnology in agriculture with major goals including better water management, optimizing nutrient application and use for increased yields, reducing release of damaging chemicals in the environment, and more efficient use of plant protection products. Here, we showed the construction of sensors, which are able to detect mRNAs related to membrane transport proteins up-regulated during Zn deficiency in plants. Most important, these sensors are portable, which means that they could be employed in the field. The principle of the sensors relies on the hybridization of mRNA target sequences with sense oligonucleotide strands attached to the surface of fluorescent upconversion nanoparticles. If the mRNA targets are bound to the upconversion nanoparticles then the particles' fluorescence is not quenched by graphene oxide indicating the presence of the target. The sensors were made portable using a detection system including a portable laser at 980 nm, a set of lenses and a smartphone camera. The sensors constructed here were successfully used to detect *OsMTP1* mRNA in RNA extracts from *OsMTP1*-transformed *Arabidopsis* and the *HvZIP5*, *HvZIP7*, *HvZIP13*, mRNAs in RNA extracts from barley grown under Zn deficiency conditions. Our study suggests strategies to create sensors for use in the field, which will benefit agriculture, informing decisions related to the nutrient status of crops.

EXPERIMENTAL METHODS

Materials. All chemicals were used as received without further purification. Erbium(III) chloride hexahydrate (99.9%), ytterbium(III) chloride hexahydrate (99.9%), yttrium(III) chloride hexahydrate (98%), ammonium fluoride (98%), methanol (99.9%), *n*-hexane (95%), poly(acrylic acid) (PAA) (MW ≈ 1.8 kDa), phosphate buffered saline tablets (PBS), 2-(*N*-morpholino) ethanesulfonic acid, 4-morpholineethanesulfonic acid (MES), sodium borate, sodium

DOI: 10.1021/acsnano.8b03261
ACS Nano 2018, 12, 6273−6279

chloride, 1-octadecene (90%), oleic acid, *N*-(3-(dimethylamino)-propyl)-N′-ethylcarbodiimide hydrochloride (EDC) (99%) and *N*-hydroxysulfosuccinimide sodium salt (Sulfo-NHS) (98%) were purchased from Sigma-Aldrich (St. Louis, MO). Tetrahydrofuran (THF), ethanol, and hexane were purchased from Fisher Scientific (Loughborough, UK) in laboratory grade. Graphene oxide (powder, flake size, 0.5−5 μm; flake thickness, 1 atomic layer−at least 80%) was purchased from Graphene Supermarket, Inc. (New York, NY). All oligonucleotide sequences for coupling to UCNPs were obtained in house (see oligonucleotides synthesis and purification). Primer sequences for PCR and RT-PCR were obtained from Integrated DNA Technologies (IDT) (Leuven, Belgium).

Methods. Transmission electron microscopy (TEM) samples were prepared by placing a drop of a diluted nanoparticle solution on a TEM copper grid coated with a Formvar film and left to dry in air. TEM images were obtained with a Hitachi HT7700 transmission electron microscope operating at a voltage of 75 kV. The nanoparticle size distribution was analyzed with ImageJ (National Institutes of Health, USA) and Soft Imaging Viewer software (Olympus, Japan), measuring over 300 nanoparticles for the statistical analysis. The upconversion fluorescence measurements were performed using a portable diode laser (Roithner Laser Technik GmbH) with continuous wave (980 nm) at 200 mW. The emitted fluorescence was collected perpendicular to the excitation beam using a 35 mm focal length lens, and was imaged onto a smartphone camera (Samsung S4). A short pass IR-blocking filter (Schott KG3) was used to suppress scattered excitation light and select only the fluorescence emission. Camera control software with manual focus, exposure, and ISO control was used to obtain images at constant exposure settings. For each measurement, 30 camera images were taken to average out variations, and the total camera intensity in the area of interest was analyzed using Matlab. A cuvette with the corresponding solvent was measured under illumination with the 980 nm laser beam and set as the blank for each measurement. The *Z*-potential measurements were performed using a Zetasizer Nano ZS instrument (Malvern Instruments, U.K.), and the accumulation time was determined automatically for each sample. The acquired data was processed using the software provided by Malvern (Zetasizer software v7.03). The UV−vis data for confirmatory experiments were acquired using a UV-2700 spectrophotometer (Shimadzu, UK). All statistics were done using ANOVA one-way with GraphPad Prism version 6.07 for Windows, GraphPad Software, La Jolla California USA, www.graphpad.com. Quantification of the emitted fluorescence for the biosensor obtained from the pictures acquired by the camera on the smartphone was performed by using Matlab on triplicates of at least 10 pictures for samples. Quantified fluorescence thresholds were set up by using the emitted fluorescence from house-keeping genes Actin as internal standard. The powder X-ray diffractions were collected using a Bruker D2 Phaser equipment with a Cu Kα (1.54 Å) X-ray source between $5° < 2\theta < 40°$.

Statistical Analysis. Two-way ANOVA was used for statistical analysis, conducted using Minitab and Prism software, with the threshold for statistical significance difference taken at a 95% confidence interval. Bonferroni, Tukey and Dunnet's posthoc tests were used as indicated to determine significant differences. Experimental measurements were taken in triplicate with at least 10 measurements each for fluorescence and photon counts. RT-PCR analyses were taken as triplicated values of technical values. Statistical analyses were conducted on SEM ± error analysis of the mean average $n = 3$.

Synthesis of Core UCNPs. The synthesis of upconversion nanocrystals was performed following a previously reported protocol with some modifications.[33] Briefly the rare earth salts, $YCl_3 \cdot 6H_2O$ (245 mg, 0.81 mmol), $YbCl_3 \cdot 6H_2O$ (107 mg, 0.28 mmol), and $ErCl_3 \cdot 6H_2O$ (15 mg, 0.04 mmol) were introduced in a 100 mL round-bottom flask. Then, oleic acid (6 mL, 19 nmol) and 1-octadecene (15 mL, 2.5 mmol) were added and the solution was heated up at 150 °C under Ar. After 1 h, the mixture was cooled down to room temperature. To this solution, a mixture of NaOH (100 mg, 2.5 mmol) and NH_4F (150 mg, 4 mmol) dissolved in 10 mL of dry MeOH were added dropwise. Then, the solution was stirred for other 30 min at room temperature and it was gradually heated up to 130 °C under Ar. After 20 min at 130 °C under Ar, it was then stirred for other 20 min at 130 °C under vacuum to ensure the complete evaporation of the MeOH. Finally, the temperature was raised to 305 °C at 15 °C/min rate under Ar and the mixture was stirred for 1 h 10 min to form the nanoparticles. After completion of the reaction, the upconversion nanoparticles were left to cool down to room temperature. EtOH (20 mL) was then added to the nanoparticles solution and the mixture was centrifuged (8000 rpm, 10 min). This process was repeated three times to purify the nanoparticles. The nanoparticles' white pellet was left to dry at 80 °C for several hours before being utilized in further experiments.

Synthesis of Core−Shell UCNPs. Core−shell nanocrystals were prepared following a previously published protocol.[28] Briefly, $YCl_3 \cdot 6H_2O$ (150 mg, 0.8 mmol) was dissolved in a solution of 1-octadecene (15 mL) and oleic acid (6 mL), and stirred for 1 h under Ar at 150 °C. The solution was cooled down to 40 °C and core UCNPs (150 mg) in $CHCl_3$ (10 mL) were added dropwise. After 20 min at 40 °C, the solution was gradually heated up to 100 °C under Ar and stirred for 45 min. Once the mixture was cooled down to room temperature under the Ar flux, a solution of NaOH (100 mg, 2.5 mmol) and NH_4F(150 mg, 4 mmol) dissolved in dry MeOH (10 mL) was added dropwise. Then, the solution was stirred for another 30 min at room temperature, and it was gradually heated up to 130 °C under Ar. After 20 min at 130 °C under Ar, it was stirred for another 20 min at 130 °C under vacuum to ensure the complete evaporation of MeOH. Finally, the temperature was raised to 305 °C at 15 °C/min rate under Ar, and the mixture was stirred for 1 h 20 min to form the core−shell UCNPs. After completion of the reaction, the nanoparticles were left to cool down to room temperature. Then, EtOH (20 mL) was added to the nanoparticles solution, and the mixture was centrifuged (8000 rpm, 10 min). This process was repeated three times to purify the nanoparticles. The core−shell UCNPs were collected as white powder and stored in $CHCl_3$.

Ligand Exchange on Core−Shell UCNPs. To bring the core−shell UCNPs in water, a ligand exchange protocol was followed to coat the nanoparticle surface with PAA.[34] In a typical reaction, PAA (0.25 g, MW ≈ 1.8 kDa) in THF (3 mL) was added to the core−shell UCNPs coated with oleic acid (21 mg in 7 mL THF). The solution was stirred for 48 h at room temperature and then centrifuged at 8000 rpm for 15 min. The particles were resuspended in THF and centrifuged again for another two times. Then the particles were suspended in EtOH (20 mL) and isolated via centrifugation (8000 rpm, 15 min) as a pellet. After drying at 80 °C for several hours, the particles were suspended in sterile DNase/RNase free Milli-Q water and stored at 4 °C.

Synthesis and Characterizations of ssDNA PAA Coated Core−Shell UCNPs. Core−shell UCNPs coated with PAA were coupled to amino-modified oligonucleotides using EDC coupling chemistry. In a typical reaction, PAA-coated UCNPs (0.5 mg mL^{-1}) were suspended in borate buffer (pH 8.5, 0.01M), and EDC (20 μL, 0.3M) and sulfo-NHS (20 μL, 0.3M) in MES buffer (pH 5.5, 0.1 M) were added. The solution was sonicated for 10 min and amine modified sense strands were added in each case [(*OsMTP1* (54.8 μL, 153.17 μM); *AtACT1* (25.6 μL, 327.20 μM); *HvZIP5* (24.5 μL, 342.94 μM); *HvZIP7* (23.5 μL, 357.05 μM); *HvZIP13* (27.8 μL, 301.78 μM); *HvACT1* (37 μL, 226.7 μM). The reaction was stirred overnight. Afterward, the particles were purified by three centrifugation steps (16400 rpm, 4 °C, 10 min). The UCNPs-ssDNA were resuspended in sterile Milli-Q and stored at −20 °C for further use.

Sensor Calibration. The sensors were calibrated in order to find the concentration of GO needed to achieve maximum quenching of core−shell UCNPs fluorescence. These experiments were carried out by adding increasing concentrations of GO (0.1−0.7 mg mL^{-1}) to a solution of a fixed concentration of ssDNA PAA-coated core−shell UCNPs (0.5 mg mL^{-1}) while measuring the fluorescence signature of the sample. It was found that 0.5 mg mL^{-1} of GO to 0.5 mg mL^{-1} of nanoparticles was the optimal ratio corresponding to the maximum quenching of the UCNPs' fluorescence (see Figure S4).

Plants Cultivation and Harvesting. *Arabidopsis thaliana* plants were grown as previously described[7,35] in soil containing equal proportions of vermiculite, Levington M2, and John Innes No. 2

DOI: 10.1021/acsnano.8b03261
ACS Nano 2018, 12, 6273−6279

compost (Fargro) in 8 cm pots; 0.28 g l-1 Intercept insecticide (Bayer, Canada) was present, and the soil was sterilized by autoclaving at 121 °C for 15 min at 1 bar pressure. Wild-type (ecotype Wassilewskija), *mtp1-1* mutant, and transgenic lines expressing OsMTP1 were grown in a controlled-environment growth room with a day/night cycle (23 °C 16 h light, 120 μmol m^{-2} s^{-1}; 18 °C 8 h dark). The T-DNA knockout *mtp1-1* mutant[36] was kindly provided by Professor Masayoshi Maeshima (Nagoya University, Japan). The *OsMTP1* gene induction in *Arabidopsis* was carried out following previous reported procedures.[2] To grow hydroponically, *Hordeum vulgare* L. cv Golden Promise seed was sterilized in 1% bleach for 15 min, rinsed in sterile water, germinated on wet tissue paper for 5 days, and then individual seedlings were grown in aerated 1 L hydroponic culture pots (Thermo Fischer Scientific, UK) in a controlled environment room (21 °C, 16 h light, 220 μmol m^{-2} s^{-1}, 55% humidity; 16 °C, 8 h dark, 65% humidity). Pots were filled with a nutrient solution (as previously described),[10] which contained 2 mM $Ca(NO_3)_2$, 1 mM KNO_3, 80 μM KH_2PO_4, 0.5 mM $MgSO_4$, 0.01 mM H_3BO_3, 0.9 mM NaOH, 75 μM $Fe(NO_3)_3$, 8.0 μM $ZnCl_2$, 0.6 μM $MnCl_2$, 2.0 μM $CuCl_2$, 0.1 μM $NiCl_2$, 0.1 μM Na_2MoO_4, and 1 mM HEDTA buffered at pH 6.0 with 1.0 mM 2-[*N*-morpholino]ethanesulfonic acid (MES). For the Zn-deficient treatment, Zn was omitted from the media. The nutrient solution was replaced every 3 days, and roots and shoots were harvested separately either for fresh weight determinations or for freezing in liquid N_2 for subsequent RNA extraction.

Isolation of RNA Extracts. Total RNA was extracted from *Arabidopsis* using Trizol Reagent according to the manufacturer's instructions (Invitrogen Life Technologies RNA, UK). RNA from hydroponically grown barley was also isolated using the Trizol method. First-strand cDNA synthesis using 1 μg of total RNA was carried out using the ImProm-IITM reverse transcriptase kit (Promega, USA) with an oligo(dT) primer according to manufacturer's instructions.

PCR Analysis in *Arabidopsis thaliana*. Standard 10 μL PCR reactions were performed using BioMix Red (Bioline), forward (F) and reverse (R) primers (Table S3) with either genomic DNA or cDNA. Reactions were performed in a peqSTAR 96 Universal PCR machine (Peqlab, Germany). For *Arabidopsis*, multiple plants were pooled from a particular genotype to generate 1 μg/μL of RNA for each biological replicate, which was then used to generate cDNA for gene expression comparisons.[4]

PCR and RT-PCR Analysis in *Hordeum vulgare*. Standard 10 μL PCR reactions were performed using BioMix Red (Bioline), forward (F) and reverse (R) primers (Table S3) with cDNA. Reactions were performed in a peqSTAR 96 Universal PCR machine (Peqlab, Germany). Real-time PCR was performed as described previously[35] with specific forward and reverse primers. For barley, tissues from three plants were pooled for each biological replicate. Gene expression levels were calculated based on previous methods,[37] standardized by normalizing to *HvACT1* for barley[2] and analyzed using Opticon software. They were expressed relative to levels of gene in Barley in the 7 days samples and within the same sample house-keeping gene. The primers sequences used for monitoring expression of a range of genes are reported in Table S2. All the forward primers were the same sequences used for PCR, Real Time PCR, and sensing detection based on the UCNPs.

ASSOCIATED CONTENT

Supporting Information

The Supporting Information is available free of charge on the ACS Publications website at DOI: 10.1021/acsnano.8b03261. The raw data is available at DOI: http://doi.org/10.5258/SOTON/D0512

Experimental procedures for the fabrication and function of the sensors, oligonucleotide sequences, further characterization of materials (PDF)

AUTHOR INFORMATION

Corresponding Author

*E-mail: a.kanaras@soton.ac.uk.

ORCID

Afaf H. El-Sagheer: 0000-0001-8706-1292
Tom Brown: 0000-0002-6538-3036
Otto L. Muskens: 0000-0003-0693-5504
Antonios G. Kanaras: 0000-0002-9847-6706

Notes

The authors declare no competing financial interest.

ACKNOWLEDGMENTS

A.G.K., O.L.M., and L.E.W. would like to thank BBSRC for funding of this project (BB/N021150/1). The Biomedical Imaging Unit at the Southampton General Hospital is also acknowledged for technical support.

REFERENCES

(1) Kumssa, D. B.; Joy, E. J. M.; Ander, E. L.; Watts, M. J.; Young, S. D.; Walker, S.; Broadley, M. R. Dietary Calcium and Zinc Deficiency Risks Are Decreasing but Remain Prevalent. *Sci. Rep.* **2015**, *5*, 10974.

(2) Mikkelsen, M. D.; Pedas, P.; Schiller, M.; Vincze, E.; Mills, R. F.; Borg, S.; Møller, A.; Schjoerring, J. K.; Williams, L. E.; Baekgaard, L.; Holm, P. B.; Palmgren, M. G. Barley HvHMA1 Is a Heavy Metal Pump Involved in Mobilizing Organellar Zn and Cu and Plays a Role in Metal Loading into Grains. *PLoS One* **2012**, *7*, e49027.

(3) Podar, D.; Scherer, J.; Noordally, Z.; Herzyk, P.; Nies, D.; Sanders, D. Metal Selectivity Determinants in a Family of Transition Metal Transporters. *J. Biol. Chem.* **2012**, *287*, 3185−3196.

(4) Menguer, P. K.; Farthing, E.; Peaston, K. A.; Ricachenevsky, F. K.; Fett, J. P.; Williams, L. E. Functional Analysis of the Rice Vacuolar Zinc Transporter OsMTP1. *J. Exp. Bot.* **2013**, *64*, 2871−2883.

(5) Menguer, P. K.; Vincent, T.; Miller, A. J.; Brown, J. K. M.; Vincze, E.; Borg, S.; Holm, P. B.; Sanders, D.; Podar, D. Improving Zinc Accumulation in Cereal Endosperm Using HvMTP1, a Transition Metal Transporter. *Plant Biotechnol. J.* **2018**, *16*, 63−71.

(6) Ricachenevsky, F. K.; Menguer, P. K.; Sperotto, R. A.; Williams, L. E.; Fett, J. P. Roles of Plant Metal Tolerance Proteins (MTP) in Metal Storage and Potential Use in Biofortification Strategies. *Front. Plant Sci.* **2013**, *4*, 144.

(7) Mills, R. F.; Peaston, K. A.; Runions, J.; Williams, L. E. HvHMA2, a P_{1B} -ATPase from Barley, Is Highly Conserved among Cereals and Functions in Zn and Cd Transport. *PLoS One* **2012**, *7*, e42640.

(8) Tiong, J.; Mcdonald, G.; Genc, Y.; Shirley, N.; Langridge, P.; Huang, C. Y. Increased Expression of Six ZIP Family Genes by Zinc (Zn) Deficiency Is Associated with Enhanced Uptake and Root-to-Shoot Translocation of Zn in Barley (*Hordeum Vulgare*). *New Phytol.* **2015**, *207*, 1097−1109.

(9) Evens, N. P.; Buchner, P.; Williams, L. E.; Hawkesford, M. J. The Role of ZIP Transporters and Group F BZIP Transcription Factors in the Zn-Deficiency Response of Wheat (*Triticum Aestivum*). *Plant J.* **2017**, *92*, 291−304.

(10) Nazri, A. Z.; Griffin, J. H. C.; Peaston, K. A.; Alexander-Webber, D. G. A.; Williams, L. E. F-group BZIPs in Barley-a Role in Zn Deficiency. *Plant, Cell Environ.* **2017**, *40*, 2754−2770.

(11) Lorenz, T. C. Polymerase Chain Reaction: Basic Protocol Plus Troubleshooting and Optimization Strategies. *J. Visualized Exp.* **2012**, *63*, e3998.

(12) Cederquist, K. B.; Keating, C. D. Hybridization Efficiency of Molecular Beacons Bound to Gold Nanowires: Effect of Surface Coverage and Target Length. *Langmuir* **2010**, *26*, 18273−18280.

(13) Kelley, S. O.; Boon, E. M.; Barton, J. K.; Jackson, N. M.; Hill, M. G. Single-Base Mismatch Detection Based on Charge Transduction through DNA. *Nucleic Acids Res.* **1999**, *27*, 4830−4837.

DOI: 10.1021/acsnano.8b03261
ACS Nano 2018, 12, 6273−6279

(14) Taton, T. A.; Lu, G.; Mirkin, C. A. Two-Color Labeling of Oligonucleotide Arrays *via* Size-Selective Scattering of Nanoparticle Probes. *J. Am. Chem. Soc.* **2001**, *123*, 5164−5165.
(15) Taton, T. A.; Mirkin, C. A.; Letsinger, R. L. Scanometric DNA Array Detection with Nanoparticle Probes. *Science* **2000**, *289*, 1757−1760.
(16) Frangioni, J. V. *In Vivo* Near-Infrared Fluorescence Imaging. *Curr. Opin. Chem. Biol.* **2003**, *7*, 626−634.
(17) Chen, Z.; Chen, H.; Hu, H.; Yu, M.; Li, F.; Zhang, Q.; Zhou, Z.; Yi, T.; Huang, C. Versatile Synthesis Strategy for Carboxylic Acid-Functionalized Upconverting Nanophosphors as Biological Labels. *J. Am. Chem. Soc.* **2008**, *130*, 3023−3029.
(18) Wang, X.; Valiev, R. R.; Ohulchanskyy, T. Y.; Ågren, H.; Yang, C.; Chen, G. Dye-Sensitized Lanthanide-Doped Upconversion Nanoparticles. *Chem. Soc. Rev.* **2017**, *46*, 4150−4167.
(19) Zhu, X.; Su, Q.; Feng, W.; Li, F. Anti-Stokes Shift Luminescent Materials for Bio-Applications. *Chem. Soc. Rev.* **2016**, *46*, 1025−1039.
(20) Alonso-Cristobal, P.; Vilela, P.; El-Sagheer, A.; Lopez-Cabarcos, E.; Brown, T.; Muskens, O. L.; Rubio-Retama, J.; Kanaras, A. G. Highly Sensitive DNA Sensor Based on Upconversion Nanoparticles and Graphene Oxide. *ACS Appl. Mater. Interfaces* **2015**, *7*, 12422−12429.
(21) Vilela, P.; El-Sagheer, A.; Millar, T. M.; Brown, T.; Muskens, O. L.; Kanaras, A. G. Graphene Oxide-Upconversion Nanoparticle Based Optical Sensors for Targeted Detection of MRNA Biomarkers Present in Alzheimer's Disease and Prostate Cancer. *ACS Sensors* **2017**, *2*, 52−56.
(22) Loh, K. P.; Bao, Q.; Eda, G.; Chhowalla, M. Graphene Oxide as a Chemically Tunable Platform for Optical Applications. *Nat. Chem.* **2010**, *2*, 1015−1024.
(23) Huang, A.; Li, W.; Shi, S.; Yao, T. Quantitative Fluorescence Quenching on Antibody-Conjugated Graphene Oxide as a Platform for Protein Sensing. *Sci. Rep.* **2017**, *7*, 1−7.
(24) Li, S.; Aphale, A. N.; MacWan, I. G.; Patra, P. K.; Gonzalez, W. G.; Miksovska, J.; Leblanc, R. M. Graphene Oxide as a Quencher for Fluorescent Assay of Amino Acids, Peptides, and Proteins. *ACS Appl. Mater. Interfaces* **2012**, *4*, 7069−7075.
(25) Liu, B.; Salgado, S.; Maheshwari, V.; Liu, J. DNA Adsorbed on Graphene and Graphene Oxide: Fundamental Interactions, Desorption and Applications. *Curr. Opin. Colloid Interface Sci.* **2016**, *26*, 41−49.
(26) Wu, M.; Kempaiah, R.; Huang, P.-J. J.; Maheshwari, V.; Liu, J. Adsorption and Desorption of DNA on Graphene Oxide Studied by Fluorescently Labeled Oligonucleotides. *Langmuir* **2011**, *27*, 2731−2738.
(27) Wang, M.; Abbineni, G.; Clevenger, A.; Mao, C.; Xu, S. Upconversion Nanoparticles: Synthesis, Surface Modification and Biological Applications. *Nanomedicine* **2011**, *7*, 710−729.
(28) Jiang, G.; Pichaandi, J.; Johnson, N. J. J.; Burke, R. D.; Van Veggel, F. C. J. M. An Effective Polymer Cross-Linking Strategy To Obtain Stable Dispersions of Upconverting NaYF4 Nanoparticles in Buffers and Biological Growth Media for Biolabeling Applications. *Langmuir* **2012**, *28*, 3239−3247.
(29) Wang, Y.; Liu, K.; Liu, X.; Dohnalová, K.; Gregorkiewicz, T.; Kong, X.; Aalders, M. C. G.; Buma, W. J.; Zhang, H. Critical Shell Thickness of Core/Shell Upconversion Luminescence Nanoplatform for Fret Application. *J. Phys. Chem. Lett.* **2011**, *2*, 2083−2088.
(30) Fischer, S.; Johnson, N. J. J.; Pichaandi, J.; Goldschmidt, J. C.; Van Veggel, F. C. J. M. Upconverting Core-Shell Nanocrystals with High Quantum Yield under Low Irradiance: On the Role of Isotropic and Thick Shells. *J. Appl. Phys.* **2015**, *118*, 193105.
(31) Shao, Q.; Zhang, G.; Ouyang, L.; Hu, Y.; Dong, Y.; Jiang, J. Emission Color Tuning of Core/Shell Upconversion Nanoparticles by Modulating the Laser Power or Temperature. *Nanoscale* **2017**, *9*, 12132−12141.
(32) Jin, J.; Gu, Y.; Man, C. W.; Cheng, J.; Xu, Z.; Zhang, Y.; Wang, H.; Lee, V. H.; Cheng, S. H.; Wong, W. Polymer-Coated $NaYF_4$:Yb^{3+}, Er^{3+} Upconversion Nanoparticles for Charge-Dependent Cellular Imaging. *ACS Nano* **2011**, *5*, 7838−7847.
(33) Li, Z.; Zhang, Y. An Efficient and User-Friendly Method for the Synthesis of Hexagonal-Phase $NaYF_4$:Yb, Er/Tm Nanocrystals with Controllable Shape and Upconversion Fluorescence. *Nanotechnology* **2008**, *19*, 345606.
(34) Lin, W.; Fritz, K.; Guerin, G.; Bardajee, G. R.; Hinds, S.; Sukhovatkin, V.; Sargent, E. H.; Scholes, G. D.; Winnik, M. A. Highly Luminescent Lead Sulfide Nanocrystals in Organic Solvents and Water through Ligand Exchange with Poly (Acrylic Acid). *Langmuir* **2008**, *24*, 8215−8219.
(35) Jaffé, F. W.; Freschet, G. C.; Valdes, B. M.; Runions, J.; Terry, M. J.; Williams, L. E. G Protein−Coupled Receptor-Type G Proteins Are Required for Light-Dependent Seedling Growth and Fertility in Arabidopsis. *Plant Cell* **2012**, *24*, 3649−3668.
(36) Kobae, Y.; Uemura, T.; Sato, M. H.; Ohnishi, M.; Mimura, T.; Maeshima, M. Zinc Transporter of Arabidopsis Thaliana AtMTP1 Is Localized to Vacuolar Membranes and Implicated in Zinc Homeostasis. *Plant Cell Physiol.* **2018**, *45*, 1749−1758.
(37) Pfaffl, M. W. A New Mathematical Model for Relative Quantification in Real-Time RT−PCR. *Nucleic Acids Res.* **2001**, *29*, 2002−2007.

DOI: 10.1021/acsnano.8b03261
ACS Nano 2018, 12, 6273−6279